Numerical Simulation and Thermal Analysis of the Filling Stage in the Injection Molding Process: Role of the Mold-Polymer Interface

Rabie El Otmani,[1] Matthieu Zinet,[1] M'hamed Boutaous,[1] Hamda Benhadid[2]

[1]*CETHIL, UMR 5008, CNRS, INSA Lyon, Université Lyon1, F-69621 Villeurbanne, France*
[2]*Laboratoire de Mécanique des Fluides et d'Acoustique, UMR 5509, CNRS, Ecole Centrale de Lyon, Université Lyon1, INSA Lyon, F-69134 Ecully, France*

Received 16 June 2010; accepted 3 November 2010
DOI 10.1002/app.33699
Published online 4 March 2011 in Wiley Online Library (wileyonlinelibrary.com).

ABSTRACT: Computer simulation is one of the most efficient ways to assist engineers to find a good design solution and to produce high quality plastic parts. The prediction of the parameter evolution during material forming requires a fair understanding of the interaction between the material properties and the process. One of the problems encountered in numerical simulation of the injection molding process is the tracking of the polymer-air front or interface during the filling stage (Haagh et al., Int Polym Proc 1997, 12, 207). This article presents a numerical simulation of a nonisothermal molten polymer flow in a cavity as in the injection molding process. The continuity and complete Navier-Stokes equations are coupled with the level set convective equation to predict the flow front and the fountain flow effect. The fluid behavior is modeled by the Cross-Arrhenius model. Thanks to the use of the level set method, a special focus is made on the polymer-mold interfacial heat transfer, and the effect of a variable thermal contact resistance is thoroughly investigated. A new interpretation of the flow marks defect causes, based on the interfacial heat flux analysis, is then suggested. © 2011 Wiley Periodicals, Inc. J Appl Polym Sci 121: 1579–1592, 2011

Key words: injection molding; rheology; computer modeling; level set method; heat transfer

INTRODUCTION

Simulation of injection molding has become an essential tool to assist the engineers in optimizing the part and mold design, as well as in identifying the most suitable process parameters for productivity and quality enhancement. So far, various kinds of models have been developed to predict the behavior of molten polymers during the filling step in the injection molding process. We can quote the pioneer works of Kamal and Kenig,[1] Tadmor et al.,[2] and Lord and Williams.[3,4] Their analyses, in simple geometries, have focused on the prediction of temperature and pressure fields. Austin[5] was then the first to extend these approaches to real parts. More recently, Coupez and coworkers[6] have proposed and implemented into the Rem3D finite element software a level set method to capture complex moving interfaces, as those occurring in fluid buckling.

Most injection-molded parts are three-dimensional, with complex geometrical configurations, and the rheological behavior of the molten polymer is generally non-Newtonian and nonisothermal.[7] Due to the several coupled phenomena and the difficulty of their numerical analysis, especially during the filling process, several simplifications are usually introduced.

Hieber and Shen,[8] using the Generalized Hele-Shaw (GHS) flow model, introduced simplified governing equations for nonisothermal and non-Newtonian flows in mold cavities. The Hele-Shaw model neglects the inertia and the gapwise velocity component for polymer melt flow in thin cavities. A review of the use of the GHS based methods can be found elsewhere.[9,10] However, because of their simplifying assumptions,[11] these models are not suitable for accurate parametric analyses. Other works[12–14] take advantage of the two-dimensional Navier-Stokes equations in Eulerian formulations. Such simplified models fail to predict the flow behavior in parts showing large curvature and complex geometries. Generally, a weak coupling between the energy and the flow equations is used, and the heat convection in the transverse direction of the flow is neglected. This leads to inaccurate predictions of the interfacial phenomena occurring between the flowing polymer and the mold.

The wavelike flow mark phenomenon is one of the surface defects that can occur in the injection

Correspondence to: M. Boutaous (mhamed.boutaous@insa-lyon.fr).

© 2011 Wiley Periodicals, Inc.

molding process. It is characterized by a part surface showing periodic hills and valleys (appearing as alternating bands of matte and gloss on the part surface) running perpendicular to the flow front direction.[15] These surface defects are commonly observed for crystalline as well as amorphous polymers, in areas where the flow front velocity is relatively low.[16]

Aiming at solving flow marks issues in injected parts, many researches have produced data concerning the influence of various molding parameters on flow mark size.[17] Simulations of the filling phase of the injection molding process have been made by Mavridis et al.[18] and show the stretching of an elementary volume of fluid with a symmetric flow front. Grillet et al.[19] have presented a study that should allow the isolation of the relevant rheological parameters effects. Their observations have demonstrated that flow marks are caused by a flow transition at the advancing molten front from a stable symmetric fountain flow to an unstable one, leading to an oscillating asymmetric flow. The two most common mechanisms that have been proposed for unstable flow are slip at the wall and instability at the point of stagnation, but so far, the origin of the instability is still unknown.

In this article, we focus our attention on the total heat flux, which is involved in a thermal explanation of the flow marks phenomenon during the filling stage. To obtain an accurate prediction of the filling flow behavior, we have combined a conservative level set method with the fully coupled continuity, momentum, and energy equations in a 2D model. A finite-element method is used to solve the set of equations. The developed model is then used to perform a parametric study. A special focus is made to analyze the effects of temperature and inlet velocity on the flow shear rate, viscosity and velocity profiles in hydrodynamically and thermally developed flows at the polymer-mold interface.

This work is divided in three sections. The first one describes the level set method applied to simulate the air-polymer front evolution during the filling process. The second one concerns the mathematical formulation and the equations governing the fluid flow and the heat transfer with specific boundary conditions. The third section is devoted to the analysis and discussion of the computational results obtained using this model, by means of a parametric study. Fountain flow, temperature profiles, density, and velocity evolutions are presented and commented. The influence of the mold interface on the heat transfer is analyzed by introducing a variable thermal contact resistance function of the nature of the fluid and the front evolution in contact with the mold walls.

THE LEVEL SET METHOD AND EQUATIONS

Several methods describing the evolution of the interface between two fluids in two phase flows exist in the literature. The level set method is a class of numerical techniques that deal with fluid interface motion. This method is particularly useful for problems in which the topology of the evolving interface changes during the course of events and for problems in which sharp corners and cusps are present.[20,21]

The level set function ϕ represents the signed distance from the interface[22] i.e., the smallest distance d between a given point in the domain and the interface:

$$|\phi(x,y)| = d(x,y) = \min_{x_\Gamma, y_\Gamma \in \Gamma} (|x - x_\Gamma|, |y - y_\Gamma|) \quad (1)$$

Following Sethian,[23] a level set function $\phi(x,y,t)$ is defined as:

$$\begin{cases} \phi(x,y,t) > 0, & (x,y) \in \Omega_1 \\ \phi(x,y,t) = 0, & (x,y) \in \Gamma \\ \phi(x,y,t) < 0, & (x,y) \in \Omega_2 \end{cases} \quad (2)$$

This function defines the interface as $\Gamma(t) = \{(x,y), \phi(x,y,t) = 0\}$ and allows us to distinguish each subdomain by the value of ϕ (Fig. 1).[24]

The evolution equation of ϕ, corresponding to the motion of the interface, is given by the convection equation:

$$\frac{\partial \phi_i}{\partial t} + u_i \frac{\partial \phi_i}{\partial x_j} = 0 \quad (3)$$

For an incompressible fluid, the continuity equation is:

$$\frac{\partial u_i}{\partial x_i} = 0 \quad (4)$$

Hence, by introducing eq. (4) in the interface convection eq. (3), the continuity equation of the level set function can be written as:

$$\frac{\partial \phi_i}{\partial t} + \frac{\partial}{\partial x_j}(u_i \phi_i) = 0 \quad (5)$$

To compute the material properties (density, heat capacity, thermal conductivity, viscosity, etc.) at the junction between the two fluids, one introduces a Heaviside function:

$$H(\phi) = \begin{cases} 0, & \phi < 0 \quad \text{(fluid 1)} \\ 1, & \phi > 0 \quad \text{(fluid 2)} \end{cases} \quad (6)$$

In numerical simulations, the abrupt jump in the material parameter values due to eq. (6) leads to instabilities when using the finite element method.

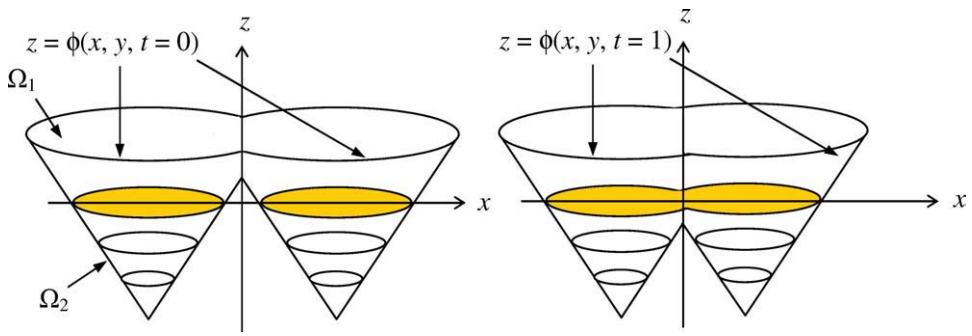

Figure 1 Representation of the level set function at two different times. [Color figure can be viewed in the online issue, which is available at wileyonlinelibrary.com].

Therefore, a smeared out Heaviside function is introduced[21]:

$$H_{sm}(\phi) = \begin{cases} 0, & \phi < -\varepsilon \\ \frac{1}{2} + \frac{\phi}{2\varepsilon} + \frac{1}{2\pi}\sin\left(\frac{\pi(\phi)}{\varepsilon}\right), & -\varepsilon \le \phi \le +\varepsilon \\ 1, & \phi > +\varepsilon \end{cases} \quad (7)$$

where ε is the half thickness of the interface or an arbitrary chosen small number, a local mesh size for instance. The interface thickness shall depend on the mesh elements size, so that it is important to mesh judiciously the domain near the interface. The variations of the thermophysical properties are then linked to ϕ. In a system made of two immiscible incompressible fluids, any additive property g can be defined by using a classical mixture law:

$$g = g_1 + (g_2 - g_1)H_{sm}(\phi) \quad (8)$$

where g_1 is defined in Ω_1 (polymer domain), and g_2 in Ω_2 (air domain).

The level set function is based on the concept of the signed distance functions.[25] To ensure the regularity of the level set function, a normalization condition must be respected during the whole advection process of ϕ:

$$\|\nabla\phi\| = 1 \quad (9)$$

Based on the computational approach proposed by Sussman and Puckett,[25] an artificial time t' is introduced to solve the initial value problem, until the steady state is reached. The steady state solution for the signed distance function ψ, in eqs. (10) and (11) at $t' = 0$ represents the level set function value:

$$\begin{cases} \frac{\partial\psi}{\partial t'} = sign(\phi(x,t))(1 - \|\nabla\psi\|) \\ \psi(x, t' = 0) = \phi(x,t) \end{cases} \quad (10)$$

Equation (10) can be rewritten as[26]:

$$\frac{\partial\psi}{\partial t'} + \left(sign(\phi(x,t))\frac{\nabla\psi}{\|\nabla\psi\|}\right).\nabla\psi = sign(\phi(x,t)) \quad (11)$$

with:

$$sign(\phi(x,t)) = \frac{\phi(x,t)}{\sqrt{(\phi(x,t))^2 + (\Delta x)^2}} \quad (12)$$

Physically, eq. (11) can be interpreted as the propagation of information away from the interface.

It is well established that the major disadvantage of the level set method is the nonconservation of mass. This represents a severe drawback, considering that inaccuracies in the mass of the polymer melt during the filling phase calculation could lead to large errors in quantities such as velocity fields, temperature, or viscosity.

To improve the mass conservation property of the level set method, sevral hybrid approaches have been proposed. Enright et al.[27] have developed a particle level set method (PLS), where Lagrangian markers are employed to correct the front location predicted by Eulerian transport. Sussman and Puckett[25] proposed to couple a level set method with the VOF technique (CLSVOF), hence benefiting from both the good mass conservation property of the VOF approach and the smooth interface description of the level set method. While both these methods have been quite successful, they suffer from additional problems. Their cost is typically much greater than the cost of a simple level set method, because many particles per cell are required for an accurate solution for the PLS approach, and because of the time step size restrictions for the geometric transport of the VOF scalar for the CLSVOF method. Moreover, the complexity of these techniques is significantly greater than that of a classical level set method.

Another attempt to alleviate the mass conservation issue of level set methods is to refine the mesh locally in order to decrease the numerical errors associated with level set transport and re-initialization. This refinement can be used for the level set equation only, such as in the case of the refined level set grid method of Herrmann,[28] or it can be a

standard arbitrary mesh refinement approach, where the Navier–Stokes equations are also solved on the refined mesh.[29] While this approach ensures a good resolution of all structures, it remains both challenging to implement on parallel systems and significantly more expensive than classical methods. Moreover, the time step size in the case of strong local refinement is likely to be extremely restrictive.

Recently, Olsson and Kreiss[20] and Olsson et al.[30] proposed a simple modification to the level set method in order to reduce mass conservation errors while retaining the simplicity of the original method. By replacing the usual signed distance function of the classical level set approach by a hyperbolic tangent profile that is transported and re-initialized using conservative equations, they showed in Olsson and Kreiss[20] that the mass conservation errors could be reduced by an order of magnitude in comparison with the results obtained with a signed distance function. In Olsson et al.,[30] the re-initialization equation is improved, and its application in the context of finite elements is discussed.

The method developed in the present work is based on the penalty approach, which consists to add in the convection equation an extra term intended to preserve the mass conservation after each time iteration:

$$\frac{\partial \phi}{\partial t} + u\nabla\phi + \beta\delta(\phi)\left(\int_{\Omega} H(\psi)d\Omega - Vol^*\right) = 0 \quad (13)$$

with β the penalty factor, *Vol** the theoretical or initial volume, and δ the Dirac function.

If the value of the penalty factor is large, the accuracy of the mass conservation is very high; however, the time resolution is increased. In the following, the performances of this method are taken advantage of for simulating the filling stage of the injection molding process. The governing equations as well as the coupling procedure with the level set equations in the finite element method are introduced and discussed in the next section.

FILLING FLOW AND HEAT TRANSFER MODEL

Nonisothermal viscous fluid flow equations

The filling phase of the injection molding process involves an incompressible, viscous, and laminar flow. In this case, the governing equations are the incompressible Navier-Stokes equation (14), the continuity equation (15) and the energy equation in the temperature form (16):

$$\rho\frac{Du_i}{Dt} = \frac{\partial}{\partial x_j}\left[\eta\left(\frac{\partial u_i}{\partial x_j} + \frac{\partial u_j}{\partial x_i}\right)\right] - \frac{\partial p}{\partial x_i} \quad (14)$$

$$\frac{\partial u_i}{\partial x_i} = 0 \quad (15)$$

$$\rho c_p\frac{DT}{Dt} = \frac{\partial}{\partial x_j}\left(k\frac{\partial T}{\partial x_j}\right) + \eta(d_{ij}d_{ji}) \quad (16)$$

where u_i are the components of the velocity vector, p is the pressure, D/Dt denotes the material derivative, η, ρ, c_p, k are respectively the viscosity, the density, the heat capacity, and the thermal conductivity of the fluid in each domain (polymer or air).

In the energy equation, the right hand terms represent the pure heat conduction in the polymer and the viscous dissipation heat source. The latter is linked to the strain-rate tensor **d** defined as:

$$d_{ij} = \frac{1}{2}\left(\frac{\partial u_i}{\partial x_j} + \frac{\partial u_j}{\partial x_i}\right) \quad (17)$$

A Cross-Arrhenius viscosity law is used to effectively describe the shear-thinning effect:

$$(T, \dot{\gamma}, p) = \frac{\eta_0(T,p)}{1 + \left(\frac{\eta_0(T,p)\dot{\gamma}}{\tau^*}\right)^{1-n}} \quad (18)$$

where n is the power-law index, τ* is the threshold shear stress at which shear thinning starts, and $\eta_0(T, p)$ the zero shear rate viscosity. The equivalent shear rate is given by:

$$\dot{\gamma} = \sqrt{2d_{ij}d_{ji}} \quad (19)$$

which, in 2D Cartesian coordinates, rewrites:

$$\dot{\gamma} = \left[2\left(\frac{\partial u}{\partial x}\right)^2 + 2\left(\frac{\partial v}{\partial y}\right)^2 + \left(\frac{\partial u}{\partial y} + \frac{\partial v}{\partial x}\right)^2\right]^{\frac{1}{2}} \quad (20)$$

The temperature dependency of the viscosity is described by the Arrhenius law:

$$\eta_0(T) = \eta_0(T_{\text{ref}})\exp\left[\frac{E_a}{R}\left(\frac{1}{T} - \frac{1}{T_{\text{ref}}}\right)\right] \quad (21)$$

It is particularly important to note that the same flow and energy equations are used for the whole injection domain, i.e., the polymer and the air flows are described by the same models. Only the physical property values explicitly depend on the fluid. The level set function locates the interface and allows the discrimination between the two fluids. This continuity of equations, variables, and properties is one of the biggest advantages of the level set method. In semicrystalline polymers, solidification, i.e., viscosity increase, not only depends on the temperature, but

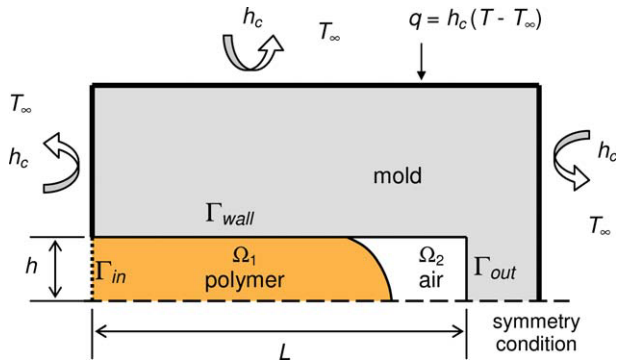

Figure 2 Geometry of the computational domain and boundary conditions. [Color figure can be viewed in the online issue, which is available at wileyonlinelibrary.com].

also on the crystallization phenomena. In this work, crystallization is not taken into account.

Flow boundary and initial conditions

On the cavity inlet Γ_{in}, (Fig. 2), a semiparabolic velocity profile is assumed:

$$\begin{cases} u(0,y,t) = \frac{3}{2}U_{\text{mean}}(1-s^2), & y \in \Gamma_{\text{in}} \\ v(0,y,t) = 0, & y \in \Gamma_{\text{in}} \end{cases} \tag{22}$$

where U_{mean} is the mean velocity of the polymer flow at the cavity inlet, and $s = y/h$ is the normalized gapwise position.

On the other boundaries, a no-slip condition is imposed for the polymer flow, and a free slip condition is prescribed downstream the polymer front for the air flow. The level set function defines the air-polymer front.

The unfilled region in the mold cavity is represented by a fictitious fluid (air). The boundary conditions on the fictitious fluid should be chosen in such a way that they have little effect on the progress of the filled region. On the air-vent (Γ_{out}), only the fictitious fluid is allowed to leave the cavity.[7,31,32–35] This condition has been incorporated by using the so-called Robin boundary condition.[31,34,35]

$$\xi u_t + \sigma_t = 0, \quad (x,y) \in \Gamma_{\text{wall}} \cup \Gamma_{\text{out}} \tag{23}$$

$$\xi u_n + \sigma_n = 0, \quad (x,y) \in \Gamma_{\text{out}} \tag{24}$$

$$u_n = 0, \quad (x,y) \in \Gamma_{\text{wall}} \tag{25}$$

The Robin penalty parameter ξ is defined as:

$$\xi = \begin{cases} 10^9, & \phi < 0 \quad \text{(no slip)} \\ 0, & \phi \geq 0 \quad \text{(free slip)} \end{cases} \tag{26}$$

u_t, σ_t, u_n, and σ_n are the velocities and the stress components in the tangential and normal directions, respectively. Since the air density and viscosity are very low compared with those of the polymer, the stresses on the interface have negligible effects on the flow. Moreover, the initial velocities in the whole computational domain have been set to zero.

Thermal boundary and initial conditions

At the mold inlet Γ_{in}, it is assumed that the polymer enters the cavity with a constant and homogeneous temperature T_{inj} (injection temperature):

$$T(0,y,t) = T_{\text{inj}} \tag{27}$$

As an initial condition for the energy equation, a uniform temperature field over the entire domain is imposed:

$$T(x,y,0) = T_0 \tag{28}$$

The heat transfer at the interface between the polymer melt and the mold is a complex phenomenon, as it depends on several parameters such as surface roughness, Young moduli of the two materials, cavity pressure, or polymer composition. Usually, as a first approximation, a perfect thermal contact is assumed between the polymer melt and the mold, leading to an overpredicted tempering effect. In this work, the imperfection of the contact is taken into account: a thermal contact resistance (TCR) between the two materials is introduced.[36] In the literature, the polymer-mold TCR have been measured (its value typically ranges between 10^{-5} and 10^{-3} m^2K/W[36,37]) and used for simulations (Sridhar,[38] Hetu et al.,[7] Guo and Narh,[39] Kamal et al.[40]). However, it should be noted that in the real process, the TCR is not constant during the whole molding cycle.

During the filling step, as the air is exhausted and replaced by the polymer melt, the heat transfer coefficient changes dynamically. It is expressed as a function of the nature of the fluid in contact with the wall, and weighted by the level set function value. In this paper, the considered values are 10^{-4} m^2K/W for the TCR at the polymer-mold contact and 100 W/m^2K for the convective heat coefficient between the air and the mold walls.

The thermal boundary condition for the heat transfer equation at the mold is written as:

$$-k\left|\frac{\partial T}{\partial y}\right| = \frac{1}{\text{TCR}}(T_{\text{wall}} - T_{\text{mold}}) \tag{29}$$

where T_{wall} is the wall temperature and k is the thermal conductivity of the polymer.

Within the mold material, pure heat conduction is assumed between the interior walls and an isothermal line corresponding to the cooling channels surface or representing the so-called thermal thickness of the mold.

TABLE I
Material Property Parameters

Parameter	Symbol	Unit	Fictitious fluid (air)	Polypropylene	Mold steel
Density	ρ	kg m^{-3}	1.199	833	7850
Constant dynamic viscosity	η	Pa s	1	–	–
Zero shear rate viscosity	η_0	Pa s		823.72	–
Cross model parameter	τ^*	Pa	–	42,419.7	–
Power law index	n	–	–	0.2614	–
Heat capacity	C_p	J kg^{-1} K^{-1}	1000	2800	475
Thermal conductivity	k	W m^{-1} K^{-1}	0.025	0.18	44.5
Initial mold temperature	T_0	K	293	–	293
Polymer injection temperature	T_{inj}	K	533	–	–
Activation energy (Arrhenius law)	E_a	J mol^{-1}	–	46,500	–
Gas constant	R	J mol^{-1} K^{-1}	8.51	–	–
Reference temperature (Arrhenius law)	T_{ref}	K	–	533	–

Moreover, a symmetry (or zero heat flux) condition is applied at the centerline of the rectangular cavity:

$$\frac{\partial T}{\partial y}(x,0,t) = 0 \tag{30}$$

Material properties

Table I summarizes the numerical values of functional parameters used in our simulation for the polypropylene (SABIC PP 86MF97) and the fictitious fluid (air).

VALIDATION OF THE MODEL

To validate the model, and to show the efficiency of the level set method to represent the flow front evolution, several tests have been performed. As it is not the aim of this article, only the validation of mass conservation and an illustration of the fountain flow are presented. The studied cavity has a thickness of 3 mm and a length of 50 mm. The computational domain is divided in two regions, as represented in Figure 2: the metallic mold and the molding cavity.

Mass conservation

Figure 3 shows the evolution of the mass loss in the mold calculated using the level set method, without any correction and after the introduction of the penalty correction developed in this work. It appears clearly that the correction is needed and the higher the penalty factor, the higher the accuracy. However, it should be precised that the calculation time is increased by about 10 when the penalty correction beta is increased from 300 to 1000.

Fountain flow

The so-called fountain flow is a characteristic pattern observed in filling flows, whose simulation can only be achieved through an accurate modeling including a front tracking method, such as the level set method presented in this article.

In mold filling, fountain flow originates from the conjugated effects of the no-slip condition at walls and the presence of the polymer-air interface. Indeed, the velocity of the fluid particles located near the flow centerline is higher than the interface velocity. Hence, as these fluid particles approach the interface, they are forced to decelerate and to be deflected toward the walls, leading to a bidimensional, stretching flow field in this zone. With respect to the flow front kinematic frame, the axial velocity of the particles becomes zero, then negative as they are drawn to the outer region of the flow, before settling at the walls to form the frozen skin layer.

The fountain flow can be clearly observed in the results of simulations performed with our model. An extra "time label" advection equation is introduced and solved together with the other equations.

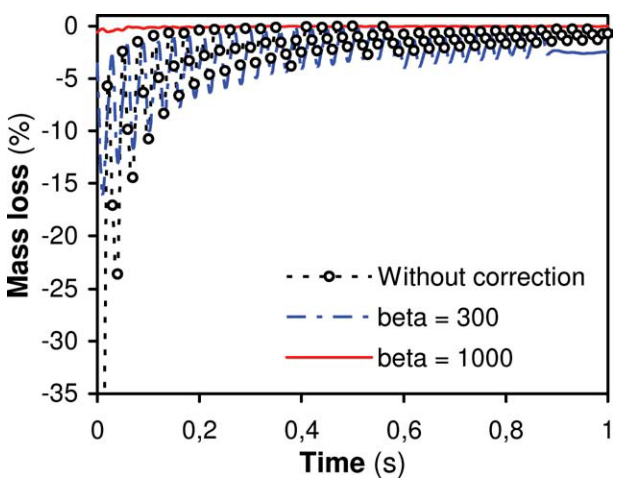

Figure 3 Validation of the mass conservation with the corrected level set method. [Color figure can be viewed in the online issue, which is available at wileyonlinelibrary.com].

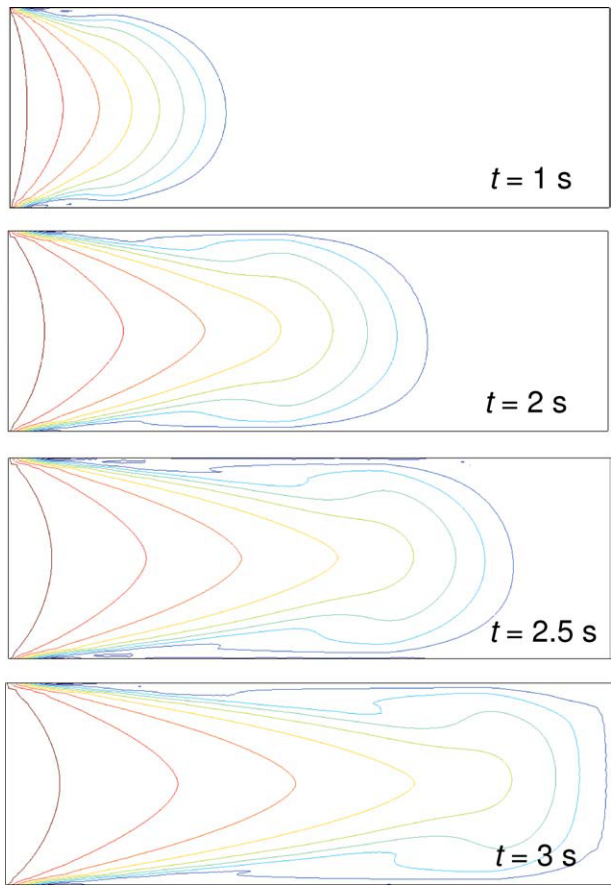

Figure 4 Fountain flow (time label isocontours) at four consecutive times of the filling stage. [Color figure can be viewed in the online issue, which is available at wileyonlinelibrary.com].

The same time label value is assigned to all the particles entering the cavity at a given time, and advected by the velocity field. The isocontour lines (Fig. 4) represent the time label distribution, i.e., the instant location of several sets of simultaneously injected particles. They can also be seen as the advection of lines, initially straight and located along the cavity inlet, by the velocity field. The isocontour lines show the typical "mushroom" shape induced by the fountain flow, as observed by Coyle et al.[41] A typical V-shaped pattern was observed from the surface to the core in a crosscut section, as reported in the works of Sato and Richardson[42] and Choi and White.[43] It is worth noticing that the particles injected in the first instants of the filling phase eventually end up along the walls, which also means that the skin layer appears very early.

The fountain flow is responsible, in large part, for the physical properties of the skin or superficial layer of injected parts. The interested reader will find more details and references concerning accurate fountain flow simulation in Behrens et al.[44] Moreover, a comparison between experimental and numerical results can be found in Rose.[45]

RESULTS AND DISCUSSION

Velocity profiles

Because of the mold-flow interactions (friction, stretching, cooling, etc.), the velocity profile evolves within the cavity, along the flow direction. Figure 5 shows the normalized velocity profile for several locations in the cavity at the end of filling time.

Obviously, the maximum velocity value is located at the centerline, but its intensity and the shape of the velocity profile changes. As a consequence, the shear rate profile also evolves along the cavity length. On one hand, the cooling of the boundary layer near the injection zone increases the viscosity, reduces the flow cross section and then accelerates the flow as imposed by the continuity and mass conservation equation. On the other hand, closer to the cavity extremity, the fluid is hotter thus less viscous. The viscous skin layer is then reduced, and the flow section increases. Hence, due to mass conservation, the maximum velocity value becomes lower.

This is particularly noticeable in Figure 6: the normalized velocity profile along the normalized cross section at the end of filling time is represented for three mean velocity values. Near the wall, the velocity is zero due to the no-slip condition, and in the central zone the velocity profile is accelerated due to the reduction of the cross-section caused by the skin layer. It can be noted that for lower mean injection velocities, the velocity value in the central zone is higher. This phenomenon is due to the solidification of the polymer skin layer contacting the mold walls. To consider the presence of the solidified layer along the mold walls, a no-flow temperature was often introduced in early studies.[46–48] However, the

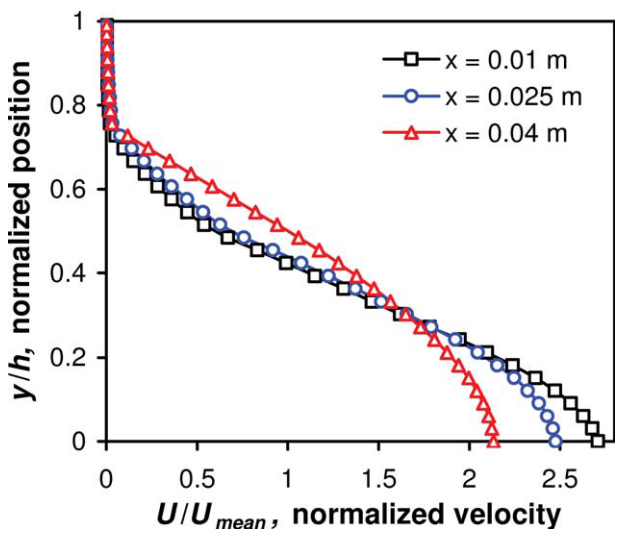

Figure 5 Gapwise velocity field at several locations along the cavity, U_{mean} = 0.02 m/s. [Color figure can be viewed in the online issue, which is available at wileyonlinelibrary.com].

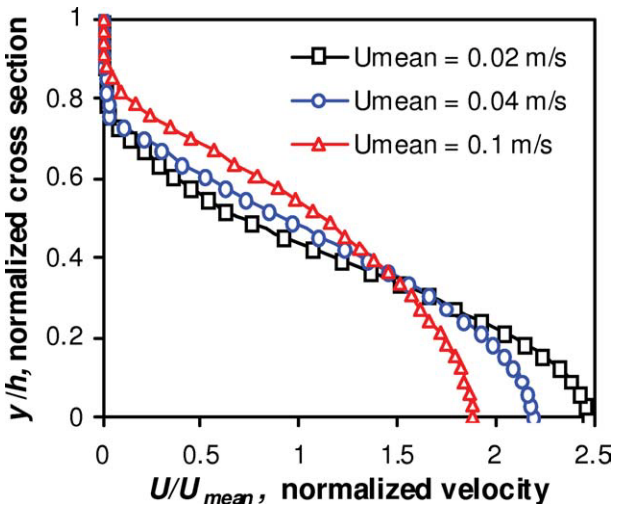

Figure 6 Normalized velocity profile in cross section $x = 0.025$ m. [Color figure can be viewed in the online issue, which is available at wileyonlinelibrary.com].

concept of no-flow temperature is difficult to define rigorously. In this study, the solidified layer is the result of the dramatic increase of viscosity expressed by the Cross-Arrhenius model used to describe the rheological behavior of the polymer melt. Thus, in the absence of crystallization, the solidified zone can be defined as the layer for which the viscosity increases by a factor of at least 10.

For higher velocities, this frozen layer is thinner because the polymer does not have enough time for cooling. At the end of filling, the polymer temperature is still high, its viscosity is then lower and the flow section larger. Such influence of the processing conditions on the velocity profile will induce different shearing histories in the flow, which in turn affects the final properties of the injected parts.

Shear rate distribution

As defined in eq. (20), once the velocity field is known, the shear rate can be calculated at any time and location in the flow domain. Figure 7 shows the predicted shear rate profile in three successive transverse sections in the cavity, for a given injection mean velocity. The normalized gapwise position s is defined as 0 at the centerline and 1 at the wall. As expected, the minimum shear rate value is found at the centerline of the cavity (symmetry), whereas the maximum value is located near the wall due to the no slip boundary condition and the formation of the skin layer. Near the cavity inlet ($x = 0.01$ m), the maximum shear rate value is higher than at the other locations ($x = 0.025$ m, $x = 0.04$ m). More precisely, it appears that the maximum shear rate in these normalized cross sections are located respectively at $s = 0.35$, $s = 0.4$, and $s = 0.6$ for $x = 0.01$ m, $x = 0.025$ m, and $x = 0.04$ m. This result shows that the thickness of the skin layer decreases as the flow moves away from the inlet zone. These displacements of the location of the maximum shear rate value can lead to the development of heterogeneous physical structures in the final part after cooling. In particular, for semicrystalline polymers, this phenomenon governs the structure gradient across the thickness of the injected parts, because the local crystallinity characteristics are directly linked to the shearing experienced by the material during flow.[49]

The influence of the injection velocity on the shear rate distributions in a cross-section located at half-length of the cavity ($x/L = 0.5$) is illustrated in Figure 8. Basically, the higher the inlet velocity, the higher the maximum shear rate. Moreover, the location of the maximum shear rate within the polymer thickness is also affected by the injection velocity. At high velocity, the polymer does not have enough time for cooling, which leads to a thinner skin layer and a maximum value of shear rate very close to the wall. This location moves toward the central zone of the polymer as the velocity decreases. When the velocity is lower, the residence time of the polymer in the cavity during filling increases and the heat transfer between the mold and the material can occur effectively. It allows the polymer to cool down before the end of filling, which leads to a thicker skin layer. The maximum shear rate is then moved towards the core zone of the injected part.

This result is meaningful as it helps to understand the link between the final structure of injected part and the processing conditions. Besides, it is known that different structural layers coexist in the thickness of injected semicrystalline thermoplastic parts. Mendoza[50] have distinguished four different layers,

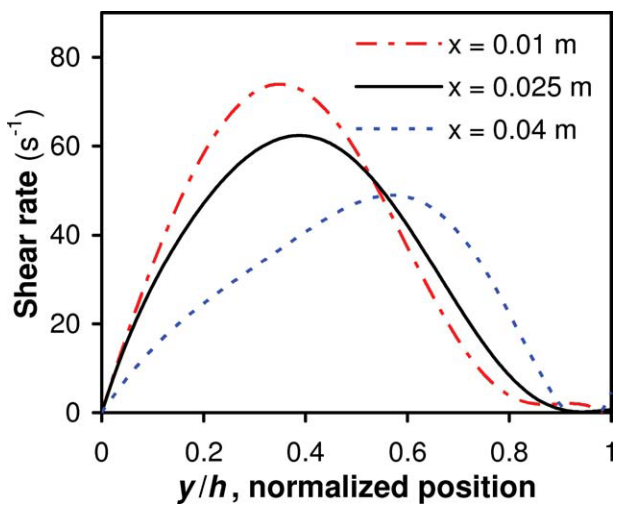

Figure 7 Shear rate profiles at the end of filling time, $U_{mean} = 0.02$ m/s. [Color figure can be viewed in the online issue, which is available at wileyonlinelibrary.com].

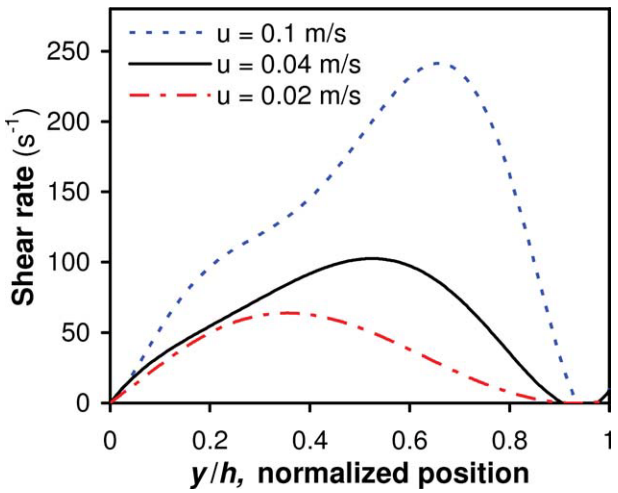

Figure 8 Shear rate profiles at the end of filling time in cross section $x/L = 0.5$. [Color figure can be viewed in the online issue, which is available at wileyonlinelibrary.com].

each one corresponding to a microstructure formed under a particular combination of processing conditions (cooling rate, pressure, shearing) during the injection molding cycle. At the end of the cooling process, this diversity of thermomechanical conditions leads to the nonhomogeneity of the final microstructure, in terms of crystallite type, density and size, as shown by Zinet et al.[51]

It is now very interesting to relate our results to these experimentally observed phenomena and facts in polymer injection molding. Figure 9 shows the evolution of the maximal shear rate value location in the part thickness during the filling stage, at several locations along the length of the cavity. A cross-sectional micrograph of an injected polypropylene part[50] is also shown for comparison.

In the near-wall zone (1), hot polymer is deflected from the central zone as a consequence of the fountain flow. Since the flow is essentially extensional, the shear rate is low and no shear orientation is induced. The elongation effect is not discussed in this paper, because, on one hand, it is not the aim of the study, and on the other hand this model can not describe it, since the polymer behavior is only represented by a generalized Newtonian rheological model. Moreover, the cooling kinetics is so fast that the material freezes immediately (tempering effect), leading to the formation of an isotropic and fine grained skin layer. The shear layer (2) corresponds to the area surrounding the maximal shear rate location shown in Figure 9. In this layer, the cooling becomes more intense, and the high shearing flow induces polymer chain orientation. These conditions result in the formation of rod-like or shish-kebab crystalline structures.[50] Finally, in the inner zones of the flow, i.e., the postfilling layer (3) and the core layer (4), the shearing is virtually inexistent and the cooling is slow due to the low thermal diffusivity of the polymer: this leads to quiescent crystallization of thermally induced, nonoriented microstructures (spherulites).

The application of our model to nonisothermal mold filling simulation provides useful information about the evolution of the processing conditions, which are known to affect the crystalline nucleation and growth mechanisms to a great extent. Therefore,

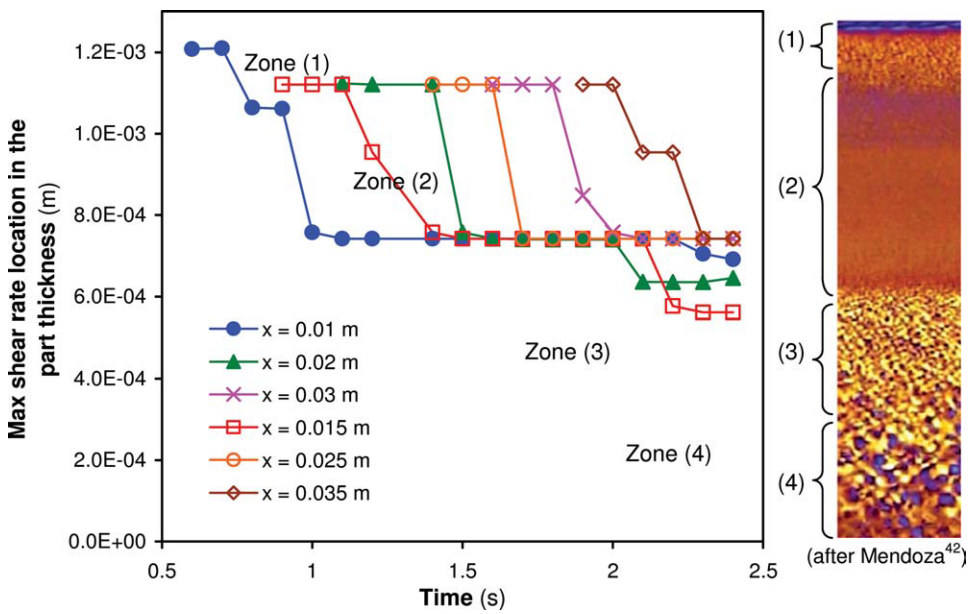

Figure 9 Evolution of the maximal shear rate value location during the filling time: comparison with experimental observation from the literature (polarized light micrograph of an injected half thickness part, after Mendoza[50]). [Color figure can be viewed in the online issue, which is available at wileyonlinelibrary.com].

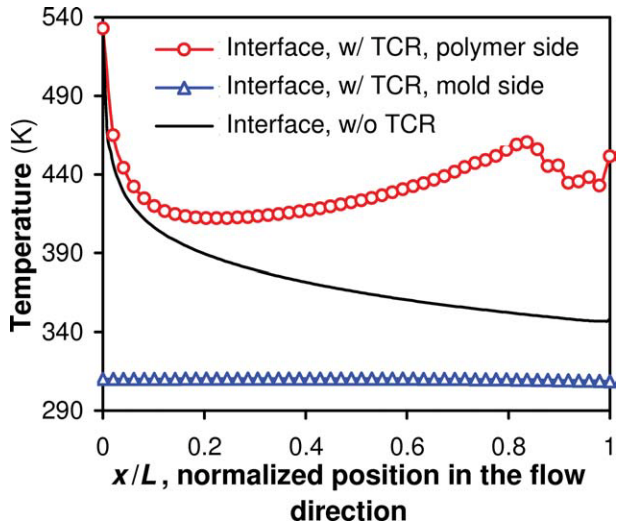

Figure 10 Mold and polymer interface temperatures evolution along the cavity length, at the end of filling time. [Color figure can be viewed in the online issue, which is available at wileyonlinelibrary.com].

the coupling of our flow model with a crystallization model[51] is promising, as it will enable the prediction of the microstructure distribution in injected parts.

Mold-polymer heat transfer analysis: importance of the TCR

It is known that the final properties of the injected parts depend on their flow and thermal histories. In this framework, one of the objectives of this article is to analyze the heat transfer phenomena that occur at the polymer-mold interface. The main idea consists in linking the flow and thermal injection conditions to some characteristics or surface defects observed on the injected polymer.

Figure 10 shows the temperature profile at the mold-polymer interface, in the flow direction, at the end of the filling time, for a given injection velocity, with and without introducing a TCR. Most of the works concerning the simulation of the injection molding process assume continuity of temperature and heat flux between the mold and the polymer. In this case, the mean temperature of the interface is given in Figure 10: at the end of the filling stage, in the inlet zone, the interface temperature reaches the polymer injection temperature. This result is not realistic because in the real process, the mold never reaches the injection temperature at any location. It is then necessary to introduce a TCR between the mold and the polymer, not only during the packing and cooling stages as usual, but also during the filling stage. The aim of this study is to prove the necessity to take into account a TCR, not to quantify it. During the injection molding cycle, the TCR evolves from a low value to a higher one, depending on the current process phase. Measuring the polymer-mold TCR value is a very difficult task; the reader interested by more details will find more details in several studies such as the important modeling work proposed by Narh,[52] or the very original experimental work of Delaunay et al.[36,37]

As an illustration, the simulation results presented in Figure 10 have been obtained with a TCR value of 10^{-4} m^2K/W. The polymer enters the cavity with a temperature $T = T_{inj} = 533$ K, and the mold is initially at $T_0 = 293$ K. The polymer temperature suddenly decreases after contacting the mold, without reaching the mold temperature. An important temperature gradient remains between the two materials, and the faster the injection velocity, the higher the temperature gradient at the mold-polymer interface, due to the condition of thermal discontinuity (TCR). At the end of the filling stage, the temperature profile on the mold interface decreases from the injection zone to the cavity extremity. Indeed, in the inlet zone, the mold has more time to diffuse heat than in the extremity zone. The inverse phenomenon is observed on the polymer side. In the extremity zone, the polymer gets in contact with a second cold wall of the mold, the bottom of the cavity (labeled Γ_{out} in Fig. 2) which explains the temperature profile decrease observed at $x/L = 0.8$.

Figure 11 focuses on the mold interface and shows the time evolution of the mold temperature for different injection velocities. The temperature decreases until the polymer front reaches the considered location. At that time, it rises suddenly because of the tempering phenomenon, then the mold diffuses heat and the temperature continues to increase with a

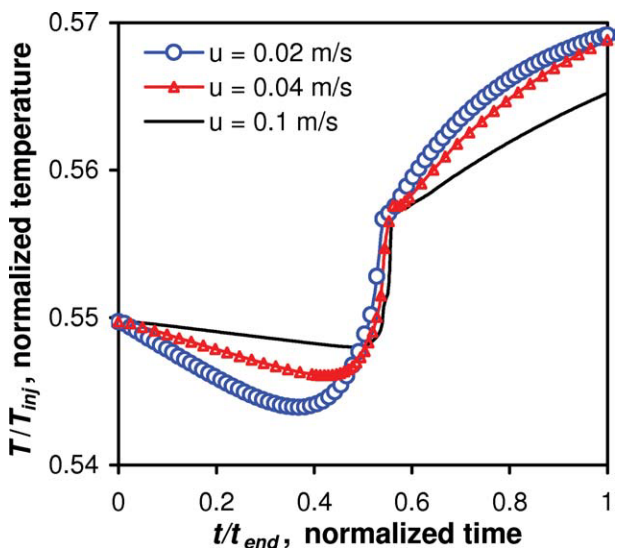

Figure 11 Evolution of the normalized interfacial temperature (mold side) at cross section. [Color figure can be viewed in the online issue, which is available at wileyonlinelibrary.com].

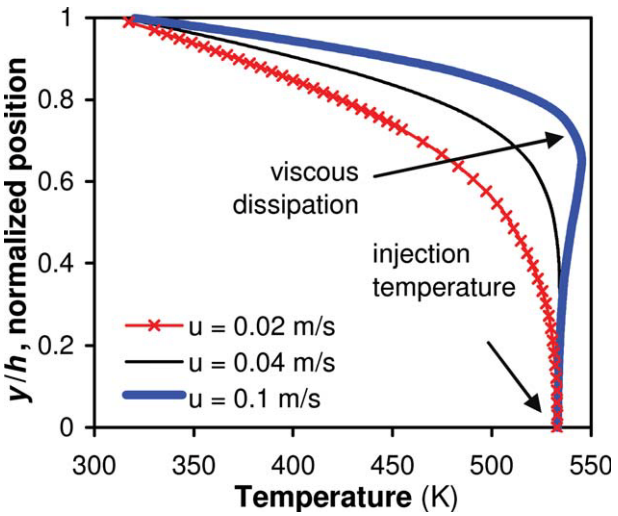

Figure 12 Gapwise temperature distribution at cross section $x/L = 0.5$, at the end of filling time, for three injection velocities. [Color figure can be viewed in the online issue, which is available at wileyonlinelibrary.com].

slower kinetics. The thermal kinetics, i.e., the slope of the curves, also depends on the mean injection velocity.

At low injection velocity, downstream the polymer front, the mold temperature is lower than at high injection velocity, because the mold is allowed to cool down for a longer time. Upstream the front, the heat extracted from the polymer is diffused in the mold. The heat diffusion time during the filling stage is longer for low velocity, and the temperature of the mold becomes higher than at higher flow velocities. The inverse phenomenon is occurring on the polymer side: a higher injection velocity leads to a higher maximum temperature value, because the polymer melt does not have enough time to cool. Note that the time is normalized by the filling time corresponding to each velocity. Indeed, at high velocity, the real injection time is lower than at low velocity.

In the injection molding process, the polymer-mold interface governs the heat transfer kinetics and has a major effect on the global thermal behavior of the polymer during all the stages of the process. Authors usually neglect heat transfer during the filling step, because it represents only a small time fraction of the whole injection cycle. However, a crucial phenomenon affecting heat transfer occurs during the filling step: the rigid polymer skin layer appears at the interface with the mold, leading to a bad interfacial thermal contact. This layer is responsible for the TCR between the mold and the polymer and also for the surface characteristics of the final injected part.

Figure 12 shows the temperature distribution across the thickness of the molding cavity, at the end of filling time, for several injection velocities. If we compare the polymer temperature for a given transverse section in the filled cavity, and for different velocities, we can say that the higher the velocity, the higher the maximum temperature value during the filling time. Moreover, at high velocity ($u = 0.1$ m/s), these curves show the self-heating phenomenon due to the viscous dissipation induced by the high shear rate: the local temperature becomes higher than the injection velocity. Basically, the frozen layer thickness depends on the local thermal conditions, which may vary during the filling phase. The amount of solidified material evolves dynamically as a result of the temperature increase due to viscous dissipation.

Heat flux distribution

A number of factors complicate the study of the polymer-mold heat transfer. First, the polymer melting and solidification often involves both a phase change and temperature dependent thermophysical properties. Moreover, due to viscous dissipation, self-heating is often generated during the filling stage. Finally, the thermal contact between the solidified polymer and the walls is not perfect (TCR). It has been shown in this article that at the flow front, the polymer melt is diverted from the center to the walls (fountain flow). As it contacts the mold walls, the melt freezes, resulting in the skin layer ("vitrified layer") of the injected part, which affects the heat transfer between the polymer and the mold. The fast solidification of the skin layer and the importance of the shear rate in this zone lead to molecular orientation, different from that in the core of the part, as explained before. The maximum value of the shear rate moves from the walls to the central zone, as the skin layer thickness increases. In this section, our purpose is to investigate the influence of the fountain flow effect on the main flow mark.

Figure 13, by Yoshii et al.,[17] illustrates the generation mechanism of the flow marks.[18] A brief description of this phenomenon may be necessary to better understand it. As the advancing front moves from A ($t = t_0$) to B ($t = t_1$), polymer particle (1) moves to the mold wall and contacts it, cools and forms solidified layer (b). So, as time elapses, the skin layer thickness increases.

For $t = t_1$ to t_2: polymer particle (1) has solidified. When the flowing front has moved to (c), the neighboring element polymer particle (2) will come into contact with the mold wall. As result, a fraction of the molten polymer will not contact the mold wall.

For $t = t_2$ to t_3: cooling of the polymer melt will advance as time has elapsed. So, fluid element (2) is larger than element (1) at mold wall. When the advancing front has moved to (D), the neighboring

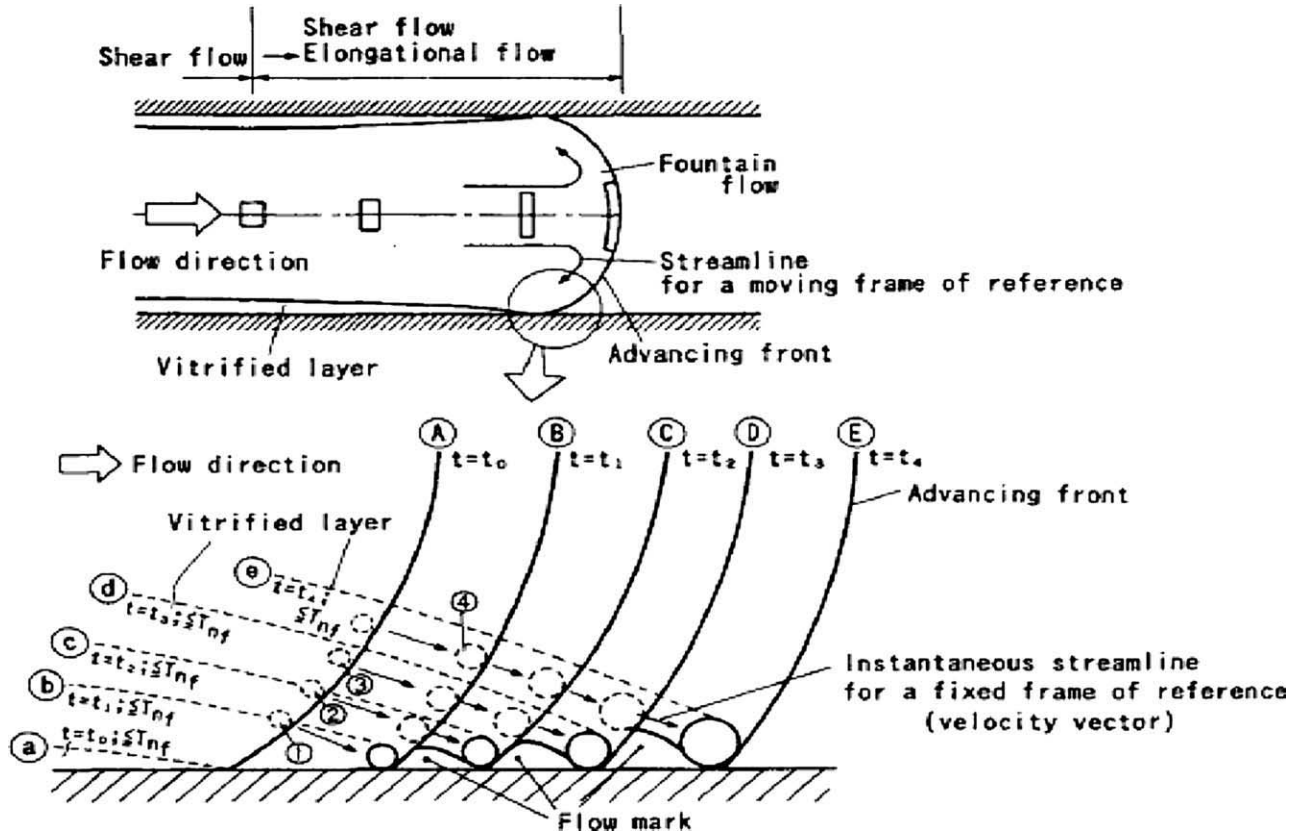

Figure 13 Nature of contact between polymer front advancing and the mold wall, after Yoshii et al.[17]

fluid element (3) will come into contact with the mold wall.

In this way, by solidification of fluid elements at the mold wall, a fraction of molten polymer will not contact the mold wall. This results in periodical roughness on the molded part surface, and can be hypothesized as the mechanism for flow mark generation.

Thanks to the accuracy of the level set method chosen to simulate the polymer front evolution, the trajectories of particles near the walls are precisely captured. Moreover, the analysis of the heat flux at the polymer-mold interface reveals an interesting phenomenon. Figure 14 shows the total interfacial heat flux for several locations along the longitudinal direction of the cavity. First, the heat flux remains zero, because the location is not yet reached by the polymer melt. When the front approaches the location, two successive peaks of the heat flux are observed. The first and lower one is due to the part of heat flux across the air trapped between the wall and the polymer front. Indeed, the polymer fluid particles are deflected by the fountain flow toward the wall, squeezing a thin air layer, and evacuating the major part of the heat flux. A fraction of this small amount of air is exhausted, while the other remains trapped, eventually causing a flow mark (Fig. 13). Because of the very small thermal conductivity of the air, the heat flux is diverted within the polymer (more conductive). In this local zone, the polymer plays a role of a thermal constriction. The major part of the heat flux follows the polymer particles, as a privileged direction.

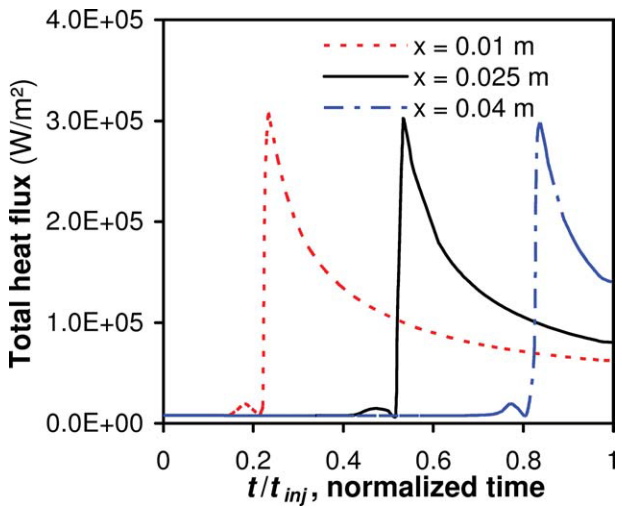

Figure 14 Evolution of the total interfacial heat flux at several locations along the cavity length. [Color figure can be viewed in the online issue, which is available at wileyonlinelibrary.com].

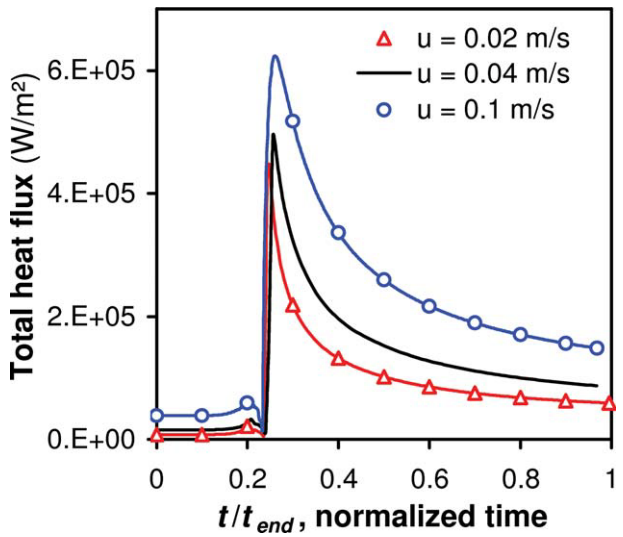

Figure 15 Evolution of the total interfacial heat flux for three injection velocities at cross section $x/L = 0.5$. [Color figure can be viewed in the online issue, which is available at wileyonlinelibrary.com].

Hence, the second heat flux peak occurs when the front contact the walls. The polymer suddenly transfers an important amount of heat to the mold, at a decaying rate as the temperature difference decreases. Figure 15 shows the same observation for several injection velocities at a given location of the polymer-mold interface. In addition, this figure shows that as the mean injection velocity decreases, the small peak decreases too. This means that for small velocities or injection rates, the flow marks tends to disappear, as observed and reported in the literature.[15,19]

This observation confirms that during the filling stage, the mold-part interface consists in a succession of contact points separated by air gaps. Therefore, it seems that a TCR should be introduced as an interfacial boundary condition during the filling stage, as done in this work.

This observation draws our attention to two types of flow marks: the micro flow marks and the macro flow marks:

The macro flow mark is generated by three factors:

1. the nature of contact between the polymer front and the mold wall surface;
2. the fountain flow effect;
3. the variation of the thickness of solidified skin layer function of the elapsed filling time.

The micro flow mark is governed by various parameters:

1. the injection velocity;
2. the injection temperature;
3. the cavity thickness;
4. the mold temperature.

The accuracy of our corrected level set method to simulate the mold-polymer interface during the filling step allows us to propose this thermal explanation of the flow marks generation. Complimentarily to the other explanations based on the mechanical behavior of the polymer at the interface or on the molecular orientation, and as proposed by some authors the polymer oscillating between the walls of the mold,[19] this suggested thermal effect constitutes an other contribution to a clear interpretation of the flow marks.

Experimental verifications are needed to confirm this observation, and very accurate and nonintrusive thermal measurements at the interface are necessary. The use of inverse methods can help to perform such measurements. Work is in progress in that perspective.

CONCLUSIONS

In this article, numerical experiments demonstrate and validate the performance of the level set method in describing interface evolution in two phase flows. This method is thus suitable for the numerical simulation of filling phase in the polymer injection molding process.

Nonisothermal transient flow of a non-Newtonian fluid in a cavity is investigated. A cross rheological model with the Arrhenius law are used as constitutive equations for the shear rate-dependant and temperature-dependant viscosity. Numerical software based on finite element method is then used to solve the coupled problem, and a parametric study of the polymer-mold interface is performed.

The simulation results have shown that the TCR between the polymer melt and the mold wall should be taken into account during the whole process, including the filling stage. Consequently, it is definitely a key parameter that needs to be determined to obtain accurate simulation results for the injection molding process.

Several additional important aspects have been analyzed. During the filling phase, the development of the solidified skin layer is strongly dependant on the TCR and other injection parameters. To quantify the effect of the TCR, all simulations have been performed considering a realistic value taken from the literature. The thickness of the skin layer at the end of filling time decreases if one of the following parameters increases: injection mean velocity, injection temperature, and TCR.

The existence of microstructure gradients in the injected part can be explained by analyzing the

location of the maximum shear rate value within the part thickness. It is shown that the polymer flow does not undergo the same thermomechanical history, depending on its position in the thickness of the part. The macromolecular chains are subjected to orientation and stretching, which in the case of semi-crystalline thermoplastics, induces strong consequences on the final part microstructure and mechanical behavior.

Moreover, the parametric analysis has underlined two major points of interest. The first one is related to the numerical validation of the developed model, tested in different configurations. The use of the suggested corrected level set method is easy and efficient for flow simulations in industrial configurations. The second one concerns the results of the interface analysis itself, which clearly shows that the filling stage in injection molding process must be systematically taken into account in the analysis of this process, because it contributes in a great extent to the determination of the final part properties, notably via the skin layer formation and the shear induced molecular orientation.

A detailed study of the solid-liquid interface has led to a better understanding of the thermal interaction between the polymer and the mold material. The interfacial heat transfer kinetics, linked to the flow behavior, shows that the heat flux can be the cause of phenomena affecting the part surface, such as aspect defects or the well-known flow mark, for which a new thermal explanation is suggested.

References

1. Kamal, M. R.; Kenig, S. Polym Eng Sci 1972, 12, 294.
2. Tadmor, Z.; Broyer, E.; Gutfinger, C. Polym Eng Sci 1974, 14, 660.
3. Lord, H. A.; Williams, G. Polym Eng Sci 1975, 15, 569.
4. Williams, G.; Lord, H. A. Polym Eng Sci 1975, 15, 553.
5. Austin, C. A. In Computer Aided Engineering for Injection Molding; Bernhardt, E. C., Ed.; Hanser: New York, 1983.
6. Ville, L.; Silva, L.; Coupez, T. Int J Numer Methods Fluids, 2010. DOI: 10.1002/fld.2259
7. Hetu, J. F.; Gao, D. M.; Garcia-Rejon, A.; Salloum, G. Polym Eng Sci 1998, 38, 223.
8. Hieber, C. A.; Shen, S. F. J Nonnewton Fluid Mech 1980, 7, 1.
9. Shen, S. F. Int J Numer Methods Eng 1992, 34, 701.
10. Tucker, C. L. Fundamentals of Computer Modeling for Polymer Processing; Hanser: Munich, Vienna, New York, 1989.
11. Kennedy, P. K. Flow Analysis of Injection Molds; Hanser: Munich, New York, 1995.
12. Anzai, K.; Niyama, E. In Modeling and Control of Casting and Welding Processes IV, Proceeding; Giamel, A. F.; Abbaschian, G. J., Eds.; TMS: Warrendale, 1988.
13. Mohammed, R. K.; Osswald, T. A.; Spiegelhoff, T. J.; Sun, E. M. Int Polym Proc 1994, 9, 279.
14. Wang, S. P. PhD Thesis, Cornell University, Ithaca, 1993.
15. Mathieu, L.; Stockmann, L.; Haudin, J. M.; Monasse, B.; Vincent, M.; Barthez, J. M.; Charmeau, J. Y.; Durand, V.; Gazonnet, J. P.; Roux, D. C. Int Polym Proc 2001, 16, 404.
16. Tredoux, L.; Satoh, I. Polym Eng Sci 2000, 40, 2161.
17. Yoshii, M.; Kuramoto, H.; Kato, K. Polym Eng Sci 1993, 33, 1251.
18. Mavridis, H.; Hrymak, A. N.; Vlachopoulos, J. Polym Eng Sci 1986, 26, 449.
19. Grillet, A. M.; Bogaerds, A. C. B.; Peters, G. W. M.; Baaijens, F. P. T. J Rheol 2002, 46, 651.
20. Olsson, E.; Kreiss, G. J Comput Phys 2005, 210, 225.
21. Sethian, J. A. Commun Math Phys 1985, 101, 487.
22. Sethian, J. A. J Diff Geom 1990, 31, 131.
23. Sethian, J. A. In Variational Methods for Free Surface Interfaces; Concus, P.; Finn, R., Eds.; Springer-Verlag: New York, 1987.
24. Sethian, J. A. PhD Thesis, Stanford University, Palo Alto, 1987.
25. Sussman, M.; Puckett, E. G. J Comput Phys 2000, 162, 301.
26. Russo, G.; Smereka, P. J Comput Phys 2000, 163, 51.
27. Enright, D.; Fedkiw, R.; Ferziger, J.; Mitchell, I. J Comput Phys 2002, 183, 83.
28. Herrmann, M. J Comput Phys 2008, 227, 2674.
29. Nourgaliev, R. R.; Theofanous, T. G. J Comput Phys 2007, 224, 836.
30. Olsson, E.; Kreiss, G.; Zahedi, S. J Comput Phys 2007, 225, 785.
31. Haagh, G. A. A. V.; Zuidema, H.; van de Vosse, F. N.; Peters, G. W. M.; Meijer, H. E. H. Int Polym Proc 1997, 12, 207.
32. Abbès, B.; Ayad, R. XIth Polyflow European Users Meeting, Bruges, 1998.
33. Abbès, B.; Ayad, R.; Rigolot, A. Revue Européenne des Eléments Finis 1999, 8, 695.
34. Haagh, G. A. A. V. PhD Thesis, Technische Universiteit, Eindhoven, 1998.
35. Haagh, G. A. A. V.; Van De Vosse, F. N. Int J Numer Methods Fluids 1998, 28, 1355.
36. Delaunay, D.; Le Bot, P.; Fulchiron, R.; Luye, J. F.; Regnier, G. Polym Eng Sci 2000, 40, 1682.
37. Delaunay, D.; Le Bot, P.; Fulchiron, R.; Luye, J. F.; Regnier, G. Polym Eng Sci 2000, 40, 1692.
38. Sridhar, L. PhD Thesis, New Jersey Institute of Technology, Newark, 1999.
39. Guo, J. X.; Narh, K. A. Polym Eng Sci 2001, 41, 1996.
40. Kamal, M. R.; Mutel, A. T.; Garcia-Rejon, A.; Salloum, G. SPE ANTEC Tech Papers 1991, 37, 438.
41. Coyle, D. J.; Blake, J. W.; Macosko, C. W. AIChE J 1987, 33, 1168.
42. Sato, T.; Richardson, S. M. Polym Eng Sci 1995, 35, 805.
43. Choi, D.; White, J. L. Int Polym Proc 2002, 17, 233.
44. Behrens, R. A.; Crochet, M. J.; Denson, C. D.; Metzner, A. B. AIChE J 1987, 33, 1178.
45. Rose, W. Nature 1961, 191, 242.
46. Pearson, J. R. A. Mechanics of Polymer Processing; Elsevier Applied Science Publishers: London, 1985.
47. Richardson, S. M. Rheol Acta 1983, 22, 223.
48. Van Wijngaarden, H.; Dijksman, J. F.; Wesseling, P. J Nonnewtonian Fluid Mech 1982, 11, 175.
49. Boutaous, M.; Bourgin, P.; Zinet, M. J Nonnewtonian Fluid Mech 2010, 165, 227.
50. Mendoza, R. PhD Thesis, ENSAM, Paris, 2005.
51. Zinet, M.; El Otmani, R.; Boutaous, M.; Chantrenne, P. Polym Eng Sci 2010, 50, 2044.
52. Narh, K. A.; Sridhar, L. SPE ANTEC Tech Papers 1997, 43, 2273.